Biochimica et Biophysica Acta 1828 (2013) 528–534

Contents lists available at SciVerse ScienceDirect

Biochimica et Biophysica Acta

journal homepage: www.elsevier.com/locate/bbamem

Peptide-induced bilayer thinning structure of unilamellar vesicles and the related binding behavior as revealed by X-ray scattering

Chun-Jen Su [a], Shiuan-Shiaou Wu [a], U-Ser Jeng [a,b,*], Ming-Tao Lee [a,c,**], An-Chung Su [b], Kuei-Fen Liao [a], Wei-Yu Lin [a], Yu-Shan Huang [a], Chun-Yu Chen [a]

[a] National Synchrotron Radiation Research Center, Hsinchu 30076, Taiwan
[b] Department of Chemical Engineering, National Tsing Hua University, Hsinchu 30013, Taiwan
[c] Department of Physics, National Central University, Jhongli 32001, Taiwan

ARTICLE INFO

Article history:
Received 19 July 2012
Received in revised form 22 October 2012
Accepted 26 October 2012
Available online 1 November 2012

Keywords:
Peptide
Membrane
Vesicle
X-ray scattering

ABSTRACT

We have studied the bilayer thinning structure of unilamellar vesicles (ULV) of a phospholipid 1,2-dierucoyl-*sn*-glycero-3-phosphocholine (di22:1PC) upon binding of melittin, a water-soluble amphipathic peptide. Successive thinning of the ULV bilayers with increasing peptide concentration was monitored via small-angle X-ray scattering (SAXS). Results suggest that the two leaflets of the ULV of closed bilayers are perturbed and thinned asymmetrically upon free peptide binding, in contrast to the centro-symmetric bilayer thinning of the substrate-oriented multilamellar membranes (MLM) with premixed melittin. Moreover, thinning of the melittin-ULV bilayer associates closely with peptide concentration in solution and saturates at ~4%, compared to the ~8% maximum thinning observed for the correspondingly premixed peptide-MLM bilayers. Linearly scaling the thinning of peptide-ULV bilayers to that of the corresponding peptide-MLM of a calibrated peptide-to-lipid ratio, we have deduced the number of bound peptides on the ULV bilayers as a function of free peptide concentration in solution. The hence derived X-ray-based binding isotherm allows extraction of a low binding constant of melittin to the ULV bilayers, on the basis of surface partition equilibrium and the Gouy–Chapman theory. Moreover, we show that the ULV and MLM bilayers of di22:1PC share a same thinning constant upon binding of a hydrophobic peptide alamethicin; this result supports the linear scaling approach used in the melittin-ULV bilayer thinning for thermodynamic binding parameters of water-soluble peptides.

1. Introduction

Membrane-active peptides with genetic codes are known to interact directly with cell membranes, rather than via specific protein receptors, in carrying out their biological functions [1–3]. In the past decades, a great variety of peptides have been shown to form transmembrane pores in cell membranes or mimic membranes of lipid vesicles [4–8]. As membrane pores are believed to be one of the primary causes for cell lysis and/or act as membrane crossing channels for ions/bio-molecules [9], understanding the pore formation process and mechanism is of broad interest. Compared to peptide activity measurements, structural studies of pores in thermodynamic equilibrium and/or formation dynamics can better address the mechanism of peptide–membrane interactions [8], as well as the regulation of ion/molecule transportation in and out of cells, thereby providing hints for drug design, disease therapy, nonviral gene transfer, and drug delivery [8,9].

Previously, membrane thinning structures upon peptide binding have been extensively studied with substrate-oriented multilamellar membranes (MLM) with premixed peptides using X-ray/neutron diffraction [5–8,10,11]. Accumulated evidences indicate that membrane thinning is, in general, a result of membrane deformation upon surface adsorption of peptides; at a critical membrane deformation (or thickness), peptides can insert into membranes and form membrane pores [6–8,12,13]. Applying contrast variation with deuterium substitution in small-angle neutron scattering [14] or Br-labeled lipid membranes in anomalous X-ray diffraction (XRD) [15], Huang et al. first illustrated peptide-induced pore structures and pore lattices in MLM and retrieved successfully the related electron density distribution [14,15]; which advanced significantly the understanding of peptide–membrane interactions.

Living cell membranes, however, comprise a single closed bilayer, and are subject to free peptides' binding in aqueous solution in certain cases. Moreover, pore formation in membranes caused by

* Corresponding author at: National Synchrotron Radiation Research Center, Hsinchu 30076, Taiwan. Tel.: +886 3 578 0281x7108; fax: +886 3 5783813.
** Corresponding author at: National Synchrotron Radiation Research Center, 101 Hsin-Ann Road, Hsinchu Science Park, Hsinchu 30076, Taiwan. Tel.: +886 3 578 0281x7109; fax: +886 3 5783813.
E-mail addresses: usjeng@nsrrc.org.tw (U.-S. Jeng), mtlee@nsrrc.org.tw (M.-T. Lee).

0005-2736/$ – see front matter © 2012 Elsevier B.V. All rights reserved.
http://dx.doi.org/10.1016/j.bbamem.2012.10.027

water-soluble amphipathic peptides typically occurs with a kinetic process [8]. Binding behavior of peptides with model membranes of single bilayer such as unilamellar vesicles (ULV) in solution would carry closer implication regarding thermodynamic or kinetic binding aspects of peptide–membrane interactions, compared to the correspondingly substrate-supported, planar peptide-MLM bilayers. Emerged recently are neutron/X-ray scattering methods that allow probing directly free-floating single bilayers of phospholipid unilamellar vesicles (ULV) in aqueous solution, in environments approaching that for real biological systems [10,11,16–19]. For instances, with neutron spin-echo spectroscopy ULV bilayers were shown to be drastically stiffened upon extensive formation of peptide-induced pores [18]. Revealed by small-angle X-ray/neutron scattering (SAXS/SANS), bilayer structures of pure phospholipid ULV bilayers were also shown to be similar (if not identical) to that of the corresponding planar MLM bilayers [10,11,17,19]. On the basis of the observations, bilayer structural changes of several phospholipids upon binding of hydrophobic alamethicin or embedment of cholesterol were revealed via integrated X-ray results obtained respectively from the ULV and MLM bilayers of the same lipids [10,11,16–19], and further complementary by molecular dynamics simulation [10,17].

In most of the ULV-based studies mentioned above, ULV bilayers were prepared with phospholipids premixed with peptides or cholesterol, of a hydrophobic nature. Nevertheless, for water-soluble amphipathic peptides, dynamic equilibrium between the peptides adsorbed to free-floating membranes and the free peptides in solution inevitably leads to a smaller peptide binding ratio onto membranes, χ_b (or P/L) than the ratio prescribed for mixing (termed as P_s/L). This should influence the bilayer thinning behavior of ULV of closed single bilayers upon water-soluble peptide binding in solution, compared to that of the corresponding substrate-supported MLM bilayers with premixed peptides. In the MLM case, kinetics of each individual bilayer may be significantly modulated by steric interactions between the stacked bilayers and further suppressed by the supporting solid substrate. Concerned here are (*i*) how a free-standing single bilayer of ULV responds to the solution binding of water-soluble amphipathic peptides and (*ii*) how binding affinity affects the dynamic equilibrium between bound peptides on the ULV bilayers and free peptides in the solution—hence the ultimate membrane thinning. Such information will not only shed lights on the underlying mechanism of water soluble peptide–membrane interactions, but also help to extract related thermodynamic parameters, such as binding constant and binding free energy [20].

In this study, using SAXS and XRD we address the two issues mentioned above by probing the bilayer thinning structures of phospholipid ULV upon solution binding of melittin, a water-soluble amphipathic peptide extracted from bee venom [8,13]. We compare the peptide-ULV bilayer thinning structures to that of the corresponding planar MLM with pre-mixed peptides, and show the similarity and dissimilarity of the ULV and MLM bilayer thinning behaviors upon binding of the same peptide. We further propose a linear scaling for the ULV bilayer thinning observed to that of MLM, to obtain the number of bound peptides. The hence established X-ray-based binding isotherm allows extraction of thermodynamic binding parameters of peptide–membrane interactions prior to membrane perforation. For an indirect support of the scaling approach used in the ULV and MLM bilayer thinning with the water-soluble melittin's binding, a hydrophobic peptide—alamethicin that can fully reside in either ULV bilayers in aqueous solution or MLM bilayers, is adopted to interact with the same model membrane [10,21]. From which result, we show that the ULV and MLM bilayers of a phospholipid 1,2-dierucoyl-*sn*-glycero-3-phosphocholine (di22:1PC) share a same bilayer thinning constant when subject to binding of the same peptide. The phospholipid di22:1PC of a long chain length was chosen for a larger thinning range. Previous studies already showed that melittin-induced membrane pores are of the toroidal type [14], differing from the barrel-stave type induced by alamethicin [22]; both peptides are known to induce transmembrane pores in lipid bilayers [12,13].

2. Materials and methods

2.1. Materials and sample preparation

Phospholipids 1,2-dierucoyl-*sn*-glycero-3-phosphocholine (di22:1PC) were purchased from Avanti Polar Lipids (Alabaster, AL). The alamethicin of purity 98% HPLC (product no. A-4665) and melittin of purity 93% HPLC (product no. M-2272) were purchased from Sigma-Aldrich Chemical Co. (St. Louis, MO). All materials were used as received without further purification. The lipids were dissolved in chloroform, dried under nitrogen flow for thin films, and then kept in vacuum for about 1 h. The lipid films were further hydrated in deionized water (pH ~ 6.8), followed by a vortex treatment for 15 min; the solutions were subjected to five rapid freeze–thaw cycles in the temperature range of −90 to 40 °C, followed by vortex-mixing for 40 min, then extruded through polycarbonate filters (with a pore size of 100 nm) at 40 °C for unilamellar vesicles. The mean diameter of the ULV determined by dynamic light scattering (Malvern Zetasizer Nano S90) was 60 nm. The aqueous solutions of di22:1PC ULV, 30–60 mM, were respectively mixed with a melittin solution for mixtures of various peptide-to-lipid ratios (P_s/L), ~10–30 min before SAXS measurements. These sample solutions were examined with preliminary SAXS measurements, ensuring no observable interference humps/peaks from residual multilamellar vesicles. For hydrophobic alamethicin, the peptide and di22:1PC were co-dissolved in solution of 1:1 v/v methanol and chloroform with several different P_s/L values (note that for hydrophobic peptides that can be fully embedded into the lipid bilayers, the mixture P_s/L is equivalent to the lipid membrane P/L). Aqueous solutions of the alamethicin-bound ULV of 30 mM were then prepared from the peptide–lipid mixtures, following the procedures used for pure di22:1PC ULV. Thin films of oriented peptide-MLM bilayers were cast onto silicon wafers from the organic solutions of different P/L; the sample films were vacuumed dried, then hydrated via water vapor.

2.2. SAXS and XRD

SAXS for the peptide-ULV solutions were conducted at the 23A SWAXS endstation of the National Synchrotron Radiation Research Center (NSRRC) [23]. With a beam of 15.0 keV (wavelength $\lambda = 0.8267$ Å) and a sample-to-detector distance of 1830 mm, SAXS data were collected using a pixel detector Pilatus-1MF of an active area of 169×179 mm^2 and a detector pixel resolution of 172 μm. This single instrument configuration could cover a reasonable q-range up to 0.5 Å^{-1} with excellent q-resolution; the scattering wavevector $q = 4\pi\lambda^{-1}\sin\theta$, defined by the scattering angle θ and λ, was calibrated with a standard sample of silver behenate. To minimize radiation damages, the 5-mm sample solution cell with thin (30 μm) quartz windows (5 mm in diameter) was gently rocked within an area of 1.5×1.5 mm^2 to avoid prolonged spot exposure (ca. 0.5 mm in beam diameter) of the sample solution at 30 °C. Each SAXS profile presented was averaged from ten SAXS data scans (each for 30 s); these ten successive scans could overlap well, suggesting negligible radiation damage effects and no structural transitions involved—hence a thermodynamically stable system. SAXS data were subtracted with water scattering measured under an identical environment as that used for the ULV sample solutions (with deionized water); the data were then corrected for incoming flux, sample thickness and electronic noise of the detector, as detailed in a previous report [23].

XRD for the peptide-bound MLM films on silicon wafers was conducted using either the 13A beamline of NSRRC with a 12 keV beam or an in-house X-ray source of 8.05 keV. The samples were respectively sealed in a humidity-controlled chamber for an environment of higher than 98% relative humidity during measurements at 30 °C [12].

2.3. Data analysis

Measured SAXS intensity profiles $I(q)$ for non-interacting ULV of little structure factor influence were modeled by the ULV form factor [24]

$$I(q) \propto \langle F(q)^2 \rangle. \quad (1)$$

Previous studies [24,25] showed that the electron density profile (EDP) $\rho(r)$ of locally flat ULV bilayers, having a radius much larger than the bilayer thickness, could be adequately approximated by a linear combination of three Gaussian functions

$$\rho(r) = \sum_{k=1}^{3} \rho_k \exp\left[-(r-\varepsilon_k)^2/\left(2\sigma_k^2\right)\right] \quad (2)$$

representing the low-electron-density region of the aliphatic chains sandwiched by the two high-electron-density regions of the phospholipid headgroups. Here, ρ_k is the amplitude of the kth Gaussian function (in relative electron density), and σ_k and ε_k and are the corresponding Gaussian distribution width and displacement from the bilayer center; for an asymmetric bilayer, values of ρ_k and σ_k may be different for the two Gaussian functions respectively representing the headgroup regions of inner and outer leaflets [24]. The scattering form factor Fourier transformed from the electron density profile (EDP) $\rho(r)$ of the bilayer is

$$F(q) = 2q^{-1}\sum_{k=1}^{3} \rho_k \sigma_k \exp\left[-\left(q^2\sigma_k^2/2\right)\right]\left[\left(\varepsilon_k \sin(q\varepsilon_k) + \sigma_k^2 q \cos(q\varepsilon_k)\right)\right] \quad (3)$$

according to Brzustowicz and Brunger [24]. Note that no phase information is needed in the model fitting of SAXS data using the form factor shown in Eqs. (1) and (3); bearing in mind that such kind of nonlinear, least-χ^2 model fitting does not provide a unique model—namely, a best-fitted model cannot exclude a possibility of an equally good one.

For diffraction data of the MLM samples, integrated peak intensities were corrected for the polarization and the Lorentz factors, then square-rooted for scattering amplitudes following that reported previously [26]. The corresponding phase of each diffraction peak was determined by the swelling method described previously [26].

3. Results and discussion

3.1. Bilayer thinning upon melittin binding

Fig. 1a shows the SAXS profiles obtained for the ULV solutions of di22:1PC mixed with melittin in aqueous solutions for different P_s/L ratios, exhibiting three clearly discernable humps of the ULV form factor scattering. Especially, the second humps of these SAXS profiles (being sensitive to the local bilayer structure, according to our model simulation) are successively asymmetrically broadened and shifted towards higher-q regions with increased P_s/L values, compared to that (centered at $q_2 = 0.282$ Å^{-1}) for pure ULV; this reveals clearly effects of peptide-induced thinning of the ULV bilayers. As proposed by Engelman [27], the distance between the two electron density peaks of the phospholipid headgroup regions (PtP) of a planar bilayer may be conveniently estimated from the center position q_2 of the second hump using $4\pi/q_2$; the PtP value thus estimated for the pure ULV bilayers is 44.5 ± 0.3 Å, which is marginally smaller than that (45.1 ± 0.3 Å) determined previously for the corresponding MLM via XRD [8]. Furthermore, shifting of the 2nd SAXS hump center for melittin-bound ULV saturates asymptotically at $P_s/L \sim 0.04$, leading to a maximum reduction of ca. 2 Å in the PtP value from that for pure ULV bilayers. The overall thinning process is qualitatively similar to that previously observed via XRD in the case of MLM bilayers (cf. Fig. S1, Supporting Information, SI) [8].

For more quantitative information we fit (dashed lines in Fig. 1a) the SAXS data using the $\rho(r)$ profiles shown in Fig. 1b, on the basis of the model described in Eqs. (1) to (3). Overall, the data and fitting curves overlap rather well, except small deviations in the high-q region ($\gtrsim 0.4$ Å^{-1}) for the higher P_s/L cases. As mentioned previously, these deviations affect marginally the fitted PtP values (in terms of the slightly larger errors shown in the inset of Fig. 2). The model with three Gaussian functions seems to describe adequately the locally flat bilayer structure of ULV, especially the PtP value that dominates the SAXS q region covering the 2nd hump. The $\rho(r)$ profiles thus obtained reveal gradually reduced PtP values from 44.0 Å of the pure ULV to a largely saturated value of 42.0 Å with $P_s/L = 0.04$ [8], as detailed in the inset of Fig. 2.

We notice that the SAXS data for the peptide-ULV could not be fitted adequately with a symmetric $\rho(r)$ profile (as illustrated in Fig. S2, SI) as that done for the pure ULV. Instead, increasingly higher asymmetry in $\rho(r)$ (Fig. 1b) is needed for fitting the SAXS profiles with increased P_s/L, having an increasingly larger asymmetry for the shape of the 2nd hump centered at $q \sim 0.28$ Å^{-1} (Fig. 1a). The symmetric $\rho(r)$ model (Fib. 1b) obtained for the pure di22:1PC ULV bilayer is consistent with the symmetric one for similar di22:1PC ULV shown by Pan et al. [10] or that for the ULV of zwitterionic dioleoyl-phosphatidylcholine (DOPC) by Kucerka et al. [19]. Whereas the fitted asymmetric $\rho(r)$ for the melittin-bound (charged) ULV of di22:1PC (Fig. 1b) is similar to the asymmetric $\rho(r)$ one reported for charged ULV of sn-1-stearoyl-sn-2-oleoyl-phosphatidylserine

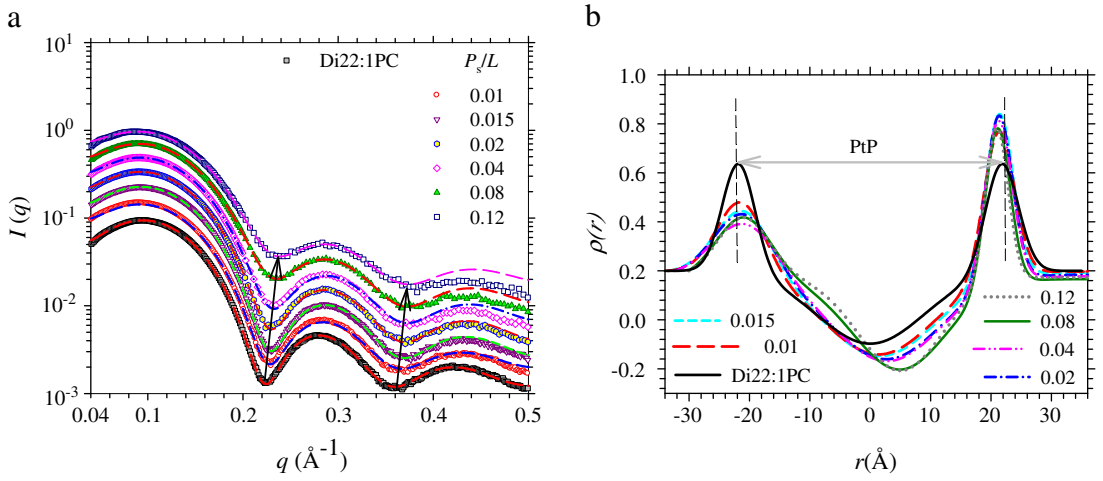

Fig. 1. SAXS profiles (a) for di22:1PC ULV mixed with melittin in water solutions for the P_s/L values indicated. The arrows outline the shifting of the 2nd SAXS hump. The data are fitted (dashed curves) using the corresponding bilayer electron density profiles in (b), with the peak-to-peak (PtP) distance marked for the pure lipid ULV bilayers.

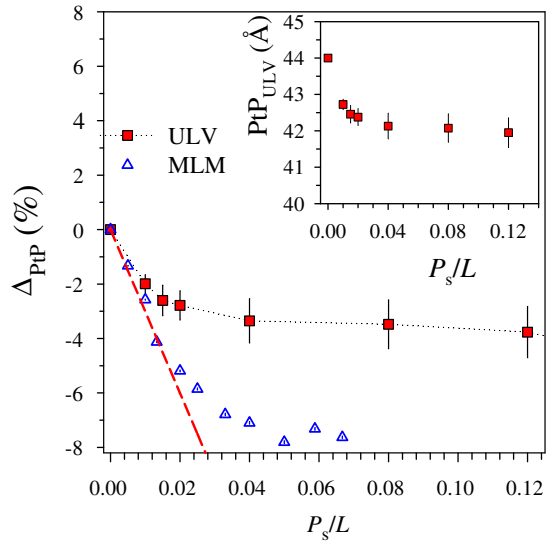

Fig. 2. Relative changes, Δ_{PtP}, in PtP for the melittin-bound ULV and MLM bilayers of di22:1PC. The Δ_{PtP} values below $P_s/L \approx 0.01$ for the MLM bilayers are fitted with a dashed line. Inset shows the corresponding PtP values of the ULV bilayers.

(SOPS) [24]. Moreover, a previous XRD study [28] for an absolute electron density profile of melittin-MLM of di22:1PC showed that a substantial increase in the electron density in the headgroup region of the bilayers could be contributed by the embedded melittin [28]. On the basis of these observations [10,28], we attribute the asymmetric $\rho(r)$ profiles as consequences of asymmetric melittin adsorption to the two leaflets of the ULV bilayers. It is likely that the outer leaflets of the ULV bilayers ($r>0$ region in Fig. 1b) facing the open solution are subject to much higher probability of peptide association and adsorption. Local association of the hydrophilic sides of the peptides with phosphate heads in the outer leaflets might result in damped thermal fluctuations, hence a sharper and higher peak in the EDP. Correspondingly, the inner leaflets facing the confined solution inside ULV would have less probability for peptide adsorption, because of a limited amount of adsorbed peptides that could enter into the ULV via transit pores before the critical P/L^* [8]. To accommodate the peptides embedded from the outer leaflets, the inner leaflets might response with tilt/slip of neighboring lipids for more hydrophobic interactions with the peptide. It is possible that without the balancing hydrophilic interactions between the peptides and the outer leaflets, the inner leaflets would suffer a large packing disorder, leading to the more broadened EDP in the $r<0$ region shown in Fig. 1b.

We note that the asymmetry revealed in the EDP profiles (Fig. 1b) does not necessary correspond to asymmetric peptide binding. Similar asymmetric bilayer $\rho(r)$ profiles for pure phospholipid ULV were reported and attributed to curvature and/or electrostatic effects [19,24]. Nevertheless, in a previous review on structure of antimicrobial peptides and lipid membranes, asymmetric peptide-binding was suggested to result in a nonuniform electron density profile across the membrane bilayer [6]; the thus induced internal stress and thinning of the membrane were associated with the mechanism of membrane pore formation previously [7,29]. Notice that the EDP profiles shown in Fig. 1b are for relative electron density. Hence, the ~30% EDP peak amplitude change near the headgroup region shown in Fig. 1b is a relative electron density change of the phosphate group region to that of the lipid chain region near the bilayer center zone. A previous report [28] indicated an increase of ~10% in absolute EDP upon melittin binding. On the basis of this result and the relative ~30% change observed here, we expect that the electron density of the lipid chains near the center of the bilayer would decrease by ~15% (owing to large disturbances of the chain packing near the central zone upon the asymmetric peptide binding, as revealed from Fig. 1b).

3.2. Linear scaling approach for binding affinity

Shown in Fig. 2 are the relative changes, Δ_{PtP}, of the PtP for melittin-ULV (or melittin-MLM) bilayers, normalized by the PtP value of pure ULV (or MLM) bilayers of di22:1PC. Scrutinizing the ULV bilayer thinning shown in Fig. 2, we notice that Δ_{PtP} values are always smaller than those of the corresponding peptide-MLM (Fig. 2) [8]. Moreover, the ULV bilayer thinning effect saturates at $\Delta_{PtP} \approx 4\%$, which is away below the critical bilayer thinning of 8% for pore formation as determined via melittin-MLM bilayers (Fig. 2). The less thinning effect of the ULV bilayers is likely originated from a finite binding affinity of the water-soluble peptide to the zwitterionic membranes in solution, leading to a peptide-to-lipid ratio of the ULV bilayers (χ_b) lower than the prescribed P_s/L for mixing. Another possible contribution to the less thinning efficiency might be from the asymmetric binding in the melittin/ULV, compared to the symmetric one in the melittin/MLM case.

Previous studies have established that MLM membrane thinning is largely linearly proportional to P/L, below the critical P/L^* value for pore formation [7,8,12,13]. In this linear thinning regime, all the peptide helices are oriented parallel to the bilayer planes for surface adsorption. Further increase of P/L above the critical P/L^* results in insertion of the surface peptides into the membrane for pore formation, leading to peptide helices perpendicular to the bilayers; and the bilayer thinning is saturated upon formation of thermal equilibrium pores [12,13]. For the peptide-MLM system, the thinning behavior below $P/L \approx 0.01$ (cf. Fig. 2) can be approximated by [12,13]

$$\Delta_{PtP} = f(P/L) \tag{4}$$

with a fitted thinning constant $f = -3.0 \pm 0.2$ (Fig. 2). It is tempting to apply this thinning constant to the reduced Δ_{PtP} measured for the peptide-ULV bilayers, and deduce the corresponding ULV χ_b value on the basis of the same linear thinning behavior defined in Eq. (4). Shown in Fig. 3 are hence obtained χ_b values, which deviate from the mixture P_s/L values increasingly more as the P_s/L ratio increases. The free peptide concentrations C_f in the solutions could be deduced from the differences between the mixture P_s/L and the deduced χ_b values, thereby establishing a quantitative correlation between the

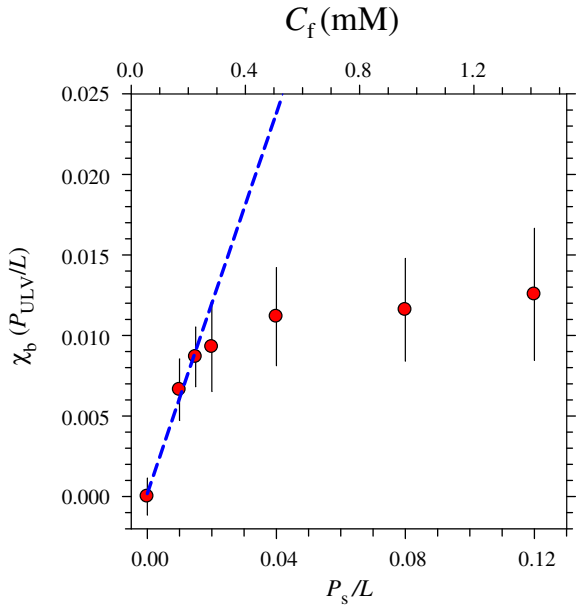

Fig. 3. P_{ULV}/L ratio for the melittin-bound di22:1PC ULV bilayers, χ_b, as a function of the prescribed P_s/L or free peptide concentration C_f (above x-axis) in the solution. The χ_b values are fitted (dashed curves) with a linear relation of $\chi_b = KC_f$ in the low C_f region ($\lesssim$0.3 mM).

bound peptides on ULV bilayers and the free peptides in solution, as a binding isotherm of melittin to di22:1PC ULV (Fig. 3). We note that the X-ray based binding isotherm is established in the regime prior to pore formation, in which the peptides are expected to mainly stay either in the solution or at the surface of (but not inserting into) the membranes.

The hence derived binding isotherm reveals an asymptotically saturated χ_b value (~0.01, corresponding to $\Delta_{PtP}\approx 4\%$) at $C_f\approx 0.3$ mM, signifying an increasing difficulty for the peptide-ULV complex in reaching the critical $\chi_b\approx 0.02$ (or $\Delta_{PtP}\approx 8\%$) for formation of thermal equilibrium pores [7,8]. Presumably, binding of charged peptides like melittin to the zwitterionic lipid membranes accumulates surface charges and gradually builds up a charge potential Ψ_0 that retards further free peptide adsorption onto the membrane, as the free peptide concentration C_f in the solution keeps increasing. As proposed previously on the basis of a surface partition equilibrium [20,21], the equilibrium χ_b may be correlated to C_f via a binding constant K (or surface partition constant) in the form of

$$\chi_b = KC_f \exp\left(-z_p F\Psi_0/RT\right) \quad (5)$$

with the effective peptide charge z_p, Faraday constant F, and thermal energy RT. On the basis of the Gouy–Chapman (GC) theory [30,31], the charge potential Ψ_0 depends on the membrane surface charge density associated with χ_b, leading to a complicate iteration relation. However, for low χ_b values with small surface charge interactions ($z_pF\Psi_0 \ll RT$ in Eq. (5)), Eq. (5) may be approximated by a linear relationship $\chi_b\approx KC_f$, allowing extraction of an approximated (underestimated) binding constant of $K = 40\ M^{-1}$ from the slope of the isotherm profile in the low C_f region as shown in Fig. 3. The small K value reflects essentially weak hydrophobic interactions of the peptide with the zwitterionic lipid membranes of di22:1PC. An apparent binding constant for melittin with charged lipid membranes, however, can be orders of magnitude higher owing to the much stronger electrostatic interactions [20,31,32]. Nevertheless, hydrophobic interactions play an intrinsic role in peptides' entering *into* membranes for pore structure [33,34], whereas high charge interactions help to increase the peptide concentration immediately above the membrane surfaces [35].

3.3. Symmetric bilayer thinning upon binding of alamethicin

In previous sections, we have illustrated the binding behavior of water soluble melittin to the ULV bilayers of di22:1PC in solution, resulting in asymmetric bilayer thinning of the membranes. There, we have assumed a common thinning factor for the di22:1PC ULV and MLM bilayers with the peptide, to establish an X-ray based binding isotherm. Since melittin is a water-soluble amphipathic peptide and will disassociate from premixed melittin-ULV bilayers according to the binding isotherm extracted (Fig. 3), we can only indirectly examine the assumption of a constant thinning factor via a hydrophobic peptide that can be fully imbedded in both MLM and ULV in a solution environment (without dissociation from premixed peptide-ULV bilayers), for quantitative comparison.

We have conducted respectively SAXS and XRD measurements for the same ULV and MLM bilayers, premixed with the hydrophobic peptide alamethicin. Shown in Fig. 4a are the SAXS results for the alamethicin-bound ULV of di22:1PC. As that discussed previously with the melittin-ULV binding, successive thinning of the ULV bilayer upon increase of the P/L value can be revealed via the broadening and shifting of the 2nd SAXS hump towards the higher-q region. Subtle differences, however, exist; the 2nd SAXS humps of the alamethicin-bound ULV bilayers are, in general, more symmetric, compared to that observed for the melittin-ULV bilayers (Fig. 1). Such feature allows fitting of the SAXS profiles with symmetric $\rho(r)$, as discussed previously [24,25]. Indeed, using the symmetric $\rho(r)$ shown in Fig. 4b, we could fit the SAXS data for alamethicin-ULV bilayers rather well (Fig. 4a). The symmetric changes in the $\rho(r)$ profiles for the two leaflets of the lipid bilayers (Fig. 4b) imply symmetric embedment of alamethicin via premixing in organic solutions.

Correspondingly obtained are the electron density profiles for the alamethicin-MLM bilayers using XRD, exhibiting a similar bilayer thinning behavior as that observed for the ULV bilayers (Fig. 5). For a more quantitative comparison, the Δ_{PtP} values deduced from the corresponding $\rho(r)$ profiles (Fig. 4b and Fig. 5b) for the peptide-bound ULV and MLM bilayers are compared. As shown in Fig. 6, these two sets of Δ_{PtP} overlap rather well, and can be fitted with a common thinning constant $f = -2.1 \pm 0.2$, according to Eq. (4). This result favors our previous assumption that both ULV and MLM share a common thinning constant, in deducing the χ_b values of the melittin-ULV bilayer of di22:1PC. The thinning factor f may be further improved for higher P/L values (>0.01), by including a non-linear thinning effect as proposed previously [36].

3.4. Comparison of the form factors of ULV and MLM bilayers of di22:1PC

We notice that the PtP values extracted for the ULV-based bilayers are systematically slightly lower (by ~1 Å) than that for the MLM-based bilayers (inset of Fig. 6). To clarify this effect, we have

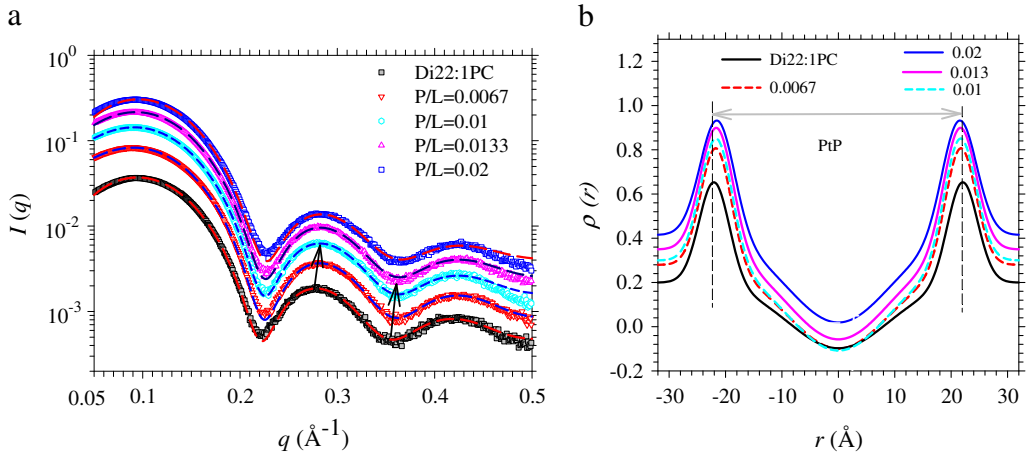

Fig. 4. SAXS profiles (a) for di22:1PC ULV solutions premixed with alamethicin for the P/L values indicated. The arrows outline the shifting of the 2nd hump towards the higher q-region from that for pure lipid ULV. The data are fitted (dashed curves) using the symmetric electron density profiles in (b). The arrow marks the PtP value of the pure lipid ULV, in contrast to the decreased PtP of the melittin-ULV bilayers.

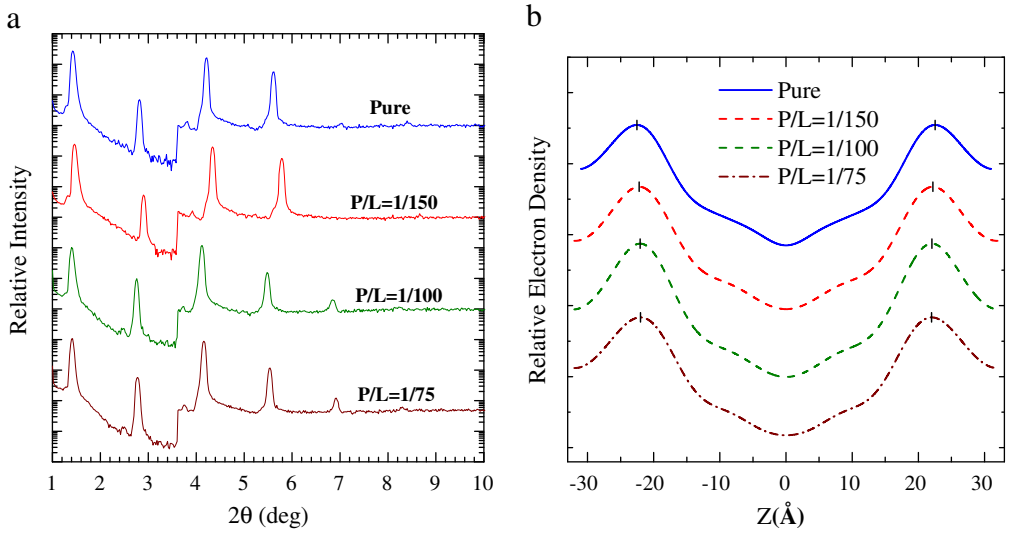

Fig. 5. (a) XRD data of the di22:1PC MLM bilayers premixed with alamethicin for the *P/L* ratios indicated. The profiles are shifted in intensity for clarity. The intensity jump near 2θ ~ 3.5° is because of an increase in incident X-ray beam intensity for improved data statistics. (b) Corresponding electron density profiles showing reduced PtP values with the increase of *P/L*.

made a direct comparison between the model independent form factor $|F(q)|$ of the ULV bilayers (data shown in Fig. 4) of di22:1PC and that of the MLM bilayers (data shown in Fig. 5), as shown in Fig. 7. The *model-independent* form factor $|F(q)|$ of the ULV bilayers is derived from the squared-root of the measured SAXS intensity profile $I(q)$, corrected for q^{-2} for phase volume [10]; whereas the form factor $|F(q_z)|$ of the MLM bilayers [17] is derived from the integral of the scattering length density profile $\rho(z)$ of the MLM bilayer of a bilayer thickness D

$$F(q_z) = \int_{-D/2}^{D/2} [\rho(z) - \rho_w] \cos(q_z z) dz \tag{6}$$

with ρ_w being the scattering length density of water. The $[\rho(z) - \rho_w]$ profile is deduced from the scattering amplitudes $F_2(h)$ of the diffraction peaks of the corresponding X-ray diffraction data for the MLM bilayer using

$$\rho(z) - \rho_w \propto \sum_h \nu_h |F_2(h)|^2 \cos(2\pi h z / D) \tag{7}$$

with the phase factor $\nu_h = +1$ or -1. Inserting the thus obtained relative electron density profile into Eq. (6) yields a reconstructed form factor of the MLM bilayers [37]

$$F(q_z) = \sum_h \nu_h |F_2(h)|^2 \mathrm{sinc}(x) \tag{8}$$

where $\mathrm{sinc}(x) = \sin(x)/x$ with $x = Dq_z/2 - h\pi$.

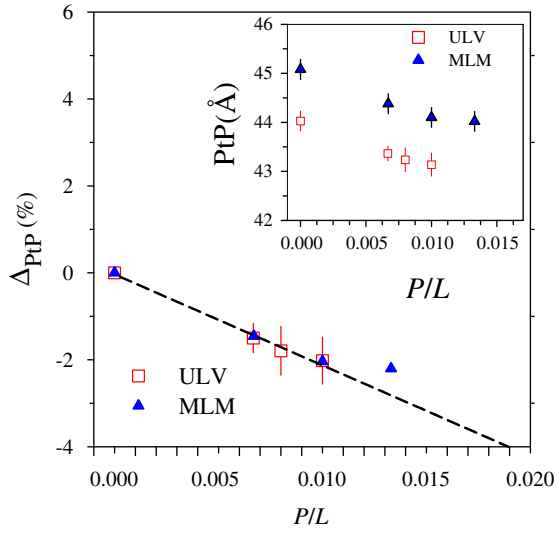

Fig. 6. Relative changes of PtP, Δ_{PtP}, of the alamethicin-bound ULV and MLM bilayers of di22:1PC. The Δ_{PtP} values below $P/L \approx 0.01$ for the MLM and ULV are fitted with a common dashed line. Inset shows the corresponding PtP values.

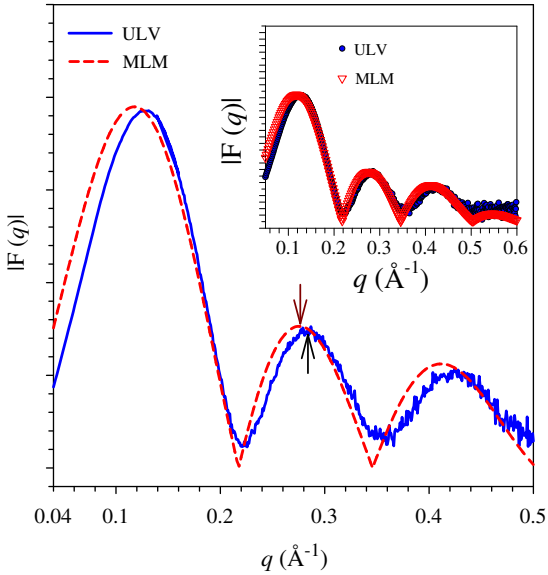

Fig. 7. Comparison of the *model-independent* form factors $|F(q)|$ of the ULV and MLM bilayers of pure di22:1PC, extracted from the data shown in Figs. 4 and 5, respectively. The form factor for the MLM bilayer shifts slightly towards the lower-*q* region relative to that for the ULV bilayer, as indicated by the arrows. Inset illustrates a general overlapping of the two form factors.

The two form factors $|F(q)|$ of UVL and MLM bilayers thus obtained illustrate a small shifting as shown in Fig. 7, which would correspond to the ~1 Å difference in the PtP values of the ULV and the MLM bilayers shown in the inset of Fig. 6. These two $|F(q)|$ profiles, nevertheless, are largely overlapped (cf. inset of Fig. 7). This model-independent comparison suggests that the revealed PtP difference in the ULV and MLM bilayers of di22:1PC should not be an artifact from the SAXS fitting model used. Rather, it might be originated from the non-identical sample environments used for the ULV and MLM bilayers. Specifically, the substrate-supported (confined) MLM bilayers were measured at a relative humidity of 98%, whereas the free-floating ULV bilayers were measured in solution subject to high thermal fluctuations. These might be responsible for the more disordered chain packing in the ULV bilayers than that in the substrate-stabilized MLM bilayers. Recent simulation studies [38,39] suggested that more disordered (or melted) bilayer packing could result in a smaller bilayer thickness. Nevertheless, the small systematic difference in the PtP values between ULV and MLM bilayers should not affect the relative PtP changes and the related conclusion made on the peptide-induced bilayer thinning behavior.

4. Conclusions

Bilayer thinning structures of the unilamellar vesicles of phospholipid di22:1PC upon solution binding of melittin are revealed using X-ray scattering techniques. The thinning of the melittin-ULV bilayers largely saturates at ~4%, whereas a maximum thinning of ~8% is observed for the melittin-MLM bilayers. The bilayer thinning observed with the hydrophobic peptide alamethicin suggests that di22:1PC ULV and MLM bilayers have a same bilayer thinning constant when subject to the same peptide binding. Via scaling the thinning of ULV bilayers to that of MLM bilayers, X-ray-based binding isotherms are established for the water-soluble amphipathic peptide, melittin, allowing extraction of thermodynamic binding parameters, such as binding constant, of peptide–membrane interactions prior to membrane perforation.

Acknowledgement

We thank Dr. Y.F. Chen for comments.

Appendix A. Supplementary data

Supplementary data to this article can be found online at http://dx.doi.org/10.1016/j.bbamem.2012.10.027.

References

[1] T. Ganz, Defensins and host defense, Science 286 (1999) 420–421.
[2] E. Martin, T. Ganz, R. Lehrer, Defensins and other endogenous peptide antibiotics of vertebrates, J. Leukoc. Biol. 58 (1995) 128–136.
[3] R. Balsa, J.M. Wilson, Cathelicidins—a family of multifunctional antimicrobial peptides, Cell. Mol. Life Sci. 60 (2003) 711–720.
[4] M. Zasloff, Antimicrobial peptides of multicellular organisms, Nature 415 (2002) 389–395.
[5] H.W. Huang, Molecular mechanism of antimicrobial peptides: the origin of cooperativity, Biochim. Biophys. Acta 1758 (2006) 1292–1302.
[6] T. Salditt, C. Li, A. Spaar, Structure of antimicrobial peptides and lipid membranes probed by interface-sensitive X-ray scattering, Biochim. Biophys. Acta 1758 (2006) 1483–1498.
[7] H.W. Huang, F.-Y. Chen, M.-T. Lee, Molecular mechanism of peptide-induced pores in membranes, Phys. Rev. Lett. 92 (2004) 198304.
[8] M.-T. Lee, W.-C. Huang, F.-Y. Chen, H.W. Huang, Mechanism and kinetics of pore formation in membranes by water-soluble amphipathic peptides, Proc. Natl. Acad. Sci. U. S. A. 105 (2008) 5087–5092.
[9] S.M. Hurtley, Crossing the bilayer, Science 310 (2005) 1451.
[10] J. Pan, D.P. Tieleman, J.F. Nagle, N. Kucerka, S. Tristram-Nagle, Alamethicin in lipid bilayers: combined use of X-ray scattering and MD simulations, Biochim. Biophys. Acta 1788 (2009) 1387–1397.
[11] N. Kucerka, J.F. Nagle, J.N. Sachs, S.E. Feller, J. Pencer, A. Jackson, J. Katsaras, Lipid bilayer structure determined by the simultaneous analysis of neutron and X-ray scattering data, Biophys. J. 95 (2008) 2356–2367.
[12] F.-Y. Chen, M.-T. Lee, H.W. Huang, Evidence for membrane thinning effect as the mechanism for peptide-induced pore formation, Biophys. J. 84 (2003) 3751–3758.
[13] M.-T. Lee, F.-Y. Chen, H.W. Huang, Energetics of pore formation induced by membrane active peptides, Biochemistry 43 (2004) 3590–3599.
[14] L. Yang, T.A. Harroun, T.M. Weiss, L. Ding, H.W. Huang, Barrel-stave model or toroidal model? A case study on melittin pores, Biophys. J. 81 (2001) 1475–1485.
[15] S. Qian, W. Wang, L. Yang, H.W. Huang, Structure of transmembrane pore induced by Bax-derived peptide: evidence for lipidic pores, Proc. Natl. Acad. Sci. 105 (2008) 17379–17383.
[16] N. Kucerka, Y. Liu, N. Chu, H.I. Petrache, S. Tristram-Nagle, J.F. Nagle, Structure of fully hydrated fluid phase DMPC and DLPC lipid bilayers using X-ray scattering from oriented multilamellar arrays and from unilamellar vesicles, Biophys. J. 88 (2005) 2626–2637.
[17] N. Kucerka, J.F. Nagle, J.N. Sachs, S.E. Feller, J. Pencer, A.J. Katsaras, Lipid bilayer structure determined by the simultaneous analysis of neutron and X-ray scattering data, Biophys. J. 95 (2008) 2356–2367.
[18] J.-H. Lee, S.-M. Choi, C. Doe, A. Faraone, P.A. Pincus, S.R. Kline, Thermal fluctuation and elasticity of lipid vesicles interacting with pore-forming peptides, Phys. Rev. Lett. 105 (2010) 038101.
[19] N. Kucerka, J. Pencer, J.N. Sachs, J.F. Nagle, J. Katsaras, Curvature effect on the structure of phospholipid bilayers, Langmuir 23 (2007) 1292–1299.
[20] G. Beschiaschvili, J. Seelig, Melittin binding to mixed phosphatidylglycerol/phosphatidylcholine membranes, Biochemistry 29 (1990) 52–58.
[21] G. Schwarz, C.H. Robert, Pore formation kinetics in membranes, determined from the release of marker molecules out of liposomes or cells, Biophys. J. 58 (1990) 577–583.
[22] S. Qian, W. Wang, L. Yang, H.W. Huang, Structure of alamethicin pore reconstructed by X-ray diffraction analysis, Biophys. J. 94 (2008) 3512–3522.
[23] U. Jeng, C.H. Su, C.-J. Su, K.-F. Liao, W.-T. Chuang, Y.-H. Lai, J.-W. Chang, Y.-J. Chen, Y.-S. Huang, M.-T. Lee, et al., A small/wide-angle X-ray scattering instrument for structural characterization of air–liquid interfaces, thin films, and bulk specimens, J. Appl. Crystallogr. 43 (2010) 110–121.
[24] M.R. Brzustowicz, A.T. Brunger, X-ray scattering from unilamellar lipid vesicles, J. Appl. Crystallogr. 38 (2005) 126–131.
[25] G. Pabst, M. Rappolt, H. Amenitsch, P. Laggner, Structural information from multilamellar liposomes at full hydration: full q-range fitting with high quality X-ray data, Phys. Rev. E. 62 (2000) 4000–4009.
[26] F.Y. Chen, W.C. Hung, H.W. Huang, Critical swelling of phospholipid bilayers, Phys. Rev. Lett. 79 (1997) 4026–4029.
[27] D.M. Engelman, Lipid bilayer structure in the membrane of Mycoplasma laidlawii, J. Mol. Biol. 58 (1971) 153–165.
[28] K. Hristova, C.E. Dempsey, S.H. White, Structure, location, and lipid perturbations of melittin at the membrane interface, Biophys. J. 80 (2001) 801–811.
[29] E. Perozo, A. Kloda, D.M. Cortes, B. Martinac, Physical principles underlying the transduction of bilayer deformation forces during mechanosensitive channel gating, Nat. Struct. Biol. 9 (2002) 696–703.
[30] S. Stankowski, Surface charging by large multivalent molecules. Extending the standard Gouy–Chapman treatment, Biophys. J. 60 (1991) 341–351.
[31] J. Seelig, S. Nebel, P. Ganz, C. Brunss, Electrostatic and nonpolar peptide–membrane interactions. Lipid binding and functional properties of somatostatin analogues of charge $z = +1$ to $z = +3$, Biochemistry 32 (1993) 9714–9721.
[32] G. Klocek, T. Schulthess, Y. Shai, J. Seelig, Thermodynamics of melittin binding to lipid bilayers. Aggregation and pore formation, Biochemistry 48 (2009) 2586–2596.
[33] H.W. Huang, Free energies of molecular bound states in lipid bilayers: lethal concentrations of antimicrobial peptides, Biophys. J. 96 (2009) 3263–3272.
[34] M. Dathe, M. Schumann, T. Wieprecht, A. Winkler, M. Beyermann, E. Krause, K. Matsuzaki, O. Murase, M. Bienert, Peptide helicity and membrane surface charge modulate the balance of electrostatic and hydrophobic interactions with lipid bilayers and biological membranes, Biochemistry 35 (1996) 12612–12622.
[35] E. Kuchinka, J. Seelig, Interaction of melittin with phosphatidylcholine membranes, Binding isotherm and lipid head-group conformation, Biochemistry 28 (1989) 4216–4221.
[36] G. Pabst, S. Danner, R. Podgornik, J. Katsaras, Entropy-driven softening of fluid lipid bilayers by alamethicin, Langmuir 23 (2007) 11705–11711.
[37] S. Aeffner, Stalk structures in lipid bilayer fusion studied by X-ray diffraction, in: Göttingen Series in X-ray Physics, volume 6, 2012, pp. 1–187, (http://www.sub.uni-goettingen.de).
[38] C.-M. Lin, C.-S. Li, Y.-J. Sheng, D.T. Wu, H.-K. Tsao, Size-dependent properties of small unilamellar vesicles formed by model lipids, Langmuir 28 (2012) 689–700.
[39] C.-M. Lin, D.T. Wu, H.-K. Tsao, Y.-J. Sheng, Membrane properties of swollen vesicles: growth, rupture, and fusion, Soft Matter 8 (2012) 6139–6150.